Available online at www.sciencedirect.com
SCIENCE DIRECT®
Sensors and Actuators A xxx (2005) xxx–xxx
SENSORS AND ACTUATORS A PHYSICAL
www.elsevier.com/locate/sna

# MEMS power generator with transverse mode thin film PZT

Y.B. Jeon [a], R. Sood [b], J.-h. Jeong [c], S.-G. Kim [d,*]

[a] *Varian Korea, KyungGi-Do, South Korea*
[b] *Polychromix, Wilmington, MA, USA*
[c] *Thin Film Materials Research Center, Korea Institute of Science and Technology, Seoul, South Korea*
[d] *Department of Mechanical Engineering, Massachusetts Institute of Technology, Cambridge, MA 02139, USA*

Accepted 17 December 2004

**Abstract**

A thin film lead zirconate titanate, $Pb(Zr,Ti)O_3$ (PZT), MEMS power generating device is developed. It is designed to resonate at specific frequencies from an external vibrational energy source, thereby creating electrical energy via the piezoelectric effect. Our cantilever device is designed to have a flat structure with a proof mass added to the end. The Pt/Ti top electrode is patterned into an interdigitated shape on top of the sol–gel-spin coated PZT thin film in order to employ the $d_{33}$ mode of the piezoelectric transducer. This $d_{33}$ mode design generates 20 times higher voltage than that of the $d_{31}$ mode design of the same beam dimension. The base-shaking experiments at the first resonant frequency (13.9 kHz) generate charge proportional to the tip displacement of the cantilever with a linearity coefficient of 4.14 pC/μm. A 170 μm × 260 μm PZT beam generates 1 μW of continuous electrical power to a 5.2 MΩ resistive load at 2.4 V dc. The corresponding energy density is 0.74 mW h/cm$^2$, which compares favorably to the values of lithium ion batteries. We expect the next generation design with lower resonant frequencies would harvest sufficient energy from the environmental vibration for wireless miniature sensor networks.


*Keywords:* Transverse mode piezoelectric; Micro power generator; Cantilever beam; Energy harvesting; interdigitated electrode

## 1. Introduction

Energy harvesting from the environment has been actively explored using several methods such as solar power, electromagnetic fields, thermal gradients, fluid flow, energy produced by the human body, and the action of gravitational fields [1]. Most of all, mechanical vibration is a potential power source which is easily accessible through microelectromechanical systems (MEMS) technology for conversion to electrical energy. The micropower energy scavenger would be ideal for tiny wireless sensors, which require self-supportive power for sensing and rf signal transfer. Recent advances in low-power VLSI design have resulted in very small power requirements of only the 10–100's of μW. This scaling trend will enable micropower energy harvesting solutions in wireless applications, eliminating the need for bulkier, higher cost, chemical batteries or wiring [2–4].

Piezoelectric materials are perfect candidates for harvesting power from ambient vibration sources because they can efficiently convert mechanical strain to an electrical charge without any additional power [5,6]. Several bulk piezoelectric generators have been developed using the $d_{31}$ piezoelectric mode [1,7,8]. But there has been no thin-film piezoelectric generator developed at the scale of MEMS. High sensitivity piezoelectric sensors have been developed recently with the transverse mode PZT, which could generate high enough open circuit voltage [9,10]. We find the use of the transverse mode PZT for power generation is beneficial to overcome the forward bias (0.2–0.3 V) of the rectifying diodes [11]. In this paper, we report a MEMS-based power generator employing the piezoelectric thin film with the $d_{33}$ mode, named as the Piezoelectric Micro Power Generator (PMPG).

* Corresponding author. Tel.: +1 617 452 2472; fax: +1 617 258 8742.
*E-mail address:* sangkim@mit.edu (S.-G. Kim).

0924-4247/$ – see front matter © 2005 Elsevier B.V. All rights reserved.
doi:10.1016/j.sna.2004.12.032

## 2. Principle and design

### 2.1. Seismic vibration of electromechanical damped mass

The energy conversion from mechanical vibration into electrical power can be described using the elements of Fig. 1 and formulated as a general model in Eq. (1) [1,12].

$$m\ddot{z}_o + (b_e + b_m)\dot{z}_o + kz_o = -m\ddot{z}_i \quad (1)$$

where $z_o$ is the device output (tip) displacement, $\ddot{z}_i$ the input (base) displacement, $m$ the lumped mass, $b_m$ the mechanical damping coefficient, $b_e$ the electrically induced damping coefficient, and $k$ is the stiffness of the MEMS device. If the system can be simplified as a linear spring damper system, the power converted to the electrical system could be given by:

$$P = \tfrac{1}{2} b_e \dot{z}_o^2 \quad (2)$$

PMPG devices should be designed so that they mechanically resonate at a frequency tuned to the ambient vibration source in order to generate maximum electrical power. The scavengeable power decreases by half if the applied frequency deviates 2% from the resonance frequency and almost goes away if the frequency deviation is more than 5% from the resonant frequency. This is why PMPG devices are modeled not as accelerometers, but as seismic devices. The resonant frequency is approximately given as $\omega_n = \sqrt{(k/m)}$ by its stiffness ($k$) and mass ($m$). Thus, the resonant frequency of the PMPG device needs to be tuned to the frequency of the ambient vibration by varying the beam dimensions and/or mass of the moving parts (i.e. layer thicknesses and the inclusion of a proof mass, if necessary). Eqs. (1) and (2) provide us with the converted power at resonance [1]:

$$|P| = \alpha\omega^3 Y^2 = \alpha\frac{A^2}{\omega} \quad (3)$$

where $\alpha = m\zeta_e/4\zeta_T^2$, $Y$ the displacement magnitude of the input vibration, $A$ the acceleration magnitude of the input vibration, $\zeta_e$ and $\zeta_T$ the electrical and total damping ratios (note that $b = 2m\omega\zeta$ where $b = b_e + b_m$ and $\zeta_T = \zeta_e + \zeta_m$). In fact, the simplified forms (Eqs. (2) and (3)) for the converted power may not be accurate enough in a piezoelectric energy conversion system when the electrical to mechanical coupling is not sufficiently linear. More accurate models will be made in the continuing research. In order to get as much power as possible, we hypothesized, at the beginning that the device needed to be operated at high frequency and have a high amplitude vibration source. According to Roundry et al. [1], however, it should be noted that the displacement amplitude and frequency are not independent in most ambient vibrational sources. The displacement amplitude decreases rapidly as the frequency goes up; that is, $Y \sim 1/w_n^2$ [1]. Considering the characteristics of the source vibration, the power decreases as frequency increases because the decreasing input vibration amplitude dominates the increasing frequency contribution. It was also found that most of the available environmental vibrations were at low frequencies. This indicates that, in order to harvest the most power from the ambient vibrations, the PMPG should resonate at a lower frequency, perhaps in the few hundred Hz. A next generation energy harvesting device, therefore, should be designed to resonate at low frequencies below several hundred Hz.

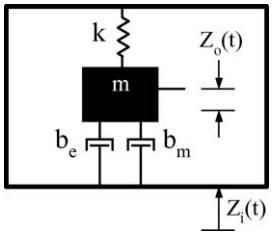


Fig. 1. Schematic of generic vibration converter.

### 2.2. Device structure

A cantilever beam structure is designed to generate a strain on the piezoelectric thin film as the beam vibrates. There are two piezoelectric modes ($d_{31}$ and $d_{33}$), which are commonly used in piezoelectric transducers. Fig. 2 is a cross-sectional view of these two piezoelectric modes. [10] They are distinguished by whether the electric field direction is perpendicular to the input strain direction ($d_{31}$) or parallel to it ($d_{33}$). Eqs. (4) and (5) show the relation between the stress $\sigma_{xx}$ (or strain $x_3$) and the electric field $E_i$ (or voltage $V_{3i}$).

$$x_3 = d_{3i}E_i \quad (4)$$

$$V_{3i} = \sigma_{xx}g_{3i}L_i \quad (5)$$

where $x_3$ is the strain, $V_{3i}$ the open circuit voltage, $d_{3i}$ (V/m) and $g_{3i}$ (Vm/N) the piezoelectric constants, and $L_i$ is the distance between electrodes which could be either $t_{PZT}$ or $L$. The $d_{3i}$ coefficient is directly proportional to $g_{3i}$ via the dielectric coefficient ($\varepsilon_{PZT}$) of the piezoelectric.

High sensitivity sensors with $d_{33}$ type piezoelectric elements were developed by Bernstein et al. [9,10] In the $d_{31}$ mode case, $L_1$ from Eq. (5) is limited to the thickness of the PZT layer $t_{pzt}$, while $L_3$ can be much longer (e.g., $\sim 10t_{pzt}$) in the $d_{33}$ case. In addition, the magnitudes of the $d_{33}$ and $g_{33}$ coefficients are 2–2.5 times higher than the $d_{31}$ and $g_{31}$ coefficients. Consequently, the generated open-circuit voltage of a $d_{33}$ type device will be much higher (20 times or greater)

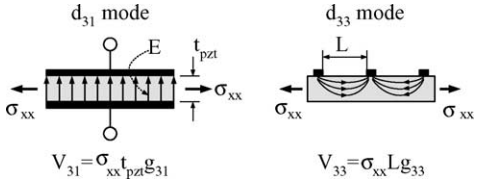


Fig. 2. Two modes of piezoelectric conversion from input mechanical stress.

than that of the $d_{31}$ type generator of similar beam dimensions, which then can overcome the forward bias of diodes (0.23 V in our rectifying system) and enables the activation of the rectifying circuit. Hence, the $d_{33}$ mode is employed to make the PZT micro cantilever device for power generation.

While the $d_{31}$ mode have separate top and bottom electrodes, the $d_{33}$ mode eliminates the need for a bottom electrode by employing an interdigitated top electrode. This also reduces the number of photo masks needed for a $d_{33}$ piezoelectric device compared with the $d_{31}$ device.

## 3. Experimental

### 3.1. Fabrication process

A piezoelectric micropower generator (PMPG) with a $d_{33}$ mode thin film lead zirconate titanate (also known as PZT) cantilever device is fabricated using three photo mask processes, as shown in Fig. 3. The structure of the PMPG is a cantilever beam consists of a membrane layer ($SiO_2$ and/or $SiN_x$), a diffusion barrier/buffer layer ($ZrO_2$) for preventing electrical charge diffusion from the piezoelectric layer, a piezoelectric thin film layer (PZT), a top interdigitated electrode (Pt/Ti), and an optional proof mass layer (SU-8).

The membrane layer is deposited on a (1 0 0) Si wafer. The warpage of the cantilever beam often found severe after the cantilever release. In order to balance the residual stress of the composite cantilever beam, three different membrane layers are deposited such as 0.4 μm thermal oxide, 0.4 μm PECVD oxide, and 0.1 μm PECVD oxide with 0.4 μm $SiN_x$. Each PECVD oxide layer is post-annealed at 750 °C for 30 min. $SiN_x$ layer of high elastic modulus (313 GPa) and tensile stress (190 MPa) is selected to have a near flat cantilever after the release. The 50 nm thick $ZrO_2$ layer is deposited via a sol–gel spin-on process over the bottom membrane, then dried at 350 °C for 1 min, and annealed at 700 °C for 15 min.

The PZT solution has a composition of Pb/(Zr + Ti) of 118/100 along with a Zr/Ti ratio of 52/48. The PZT solution is spun on the substrate at 500 rpm for 3 s and 1500 rpm for 30 s. The precursor gel film is pyrolyzed at 350 °C for 5 min on a hot plate. This deposition process cycle is repeated four times to make a PZT layer of 0.48 μm thickness. The PZT film is then annealed at 700 °C for 15 min. The PZT layer and membrane layers are patterned via RIE with $BCl_3$:$Cl_2$ (30:10) gas chemistry for 70 min with the first etch mask. The top interdigitated electrode is deposited next with 20 nm

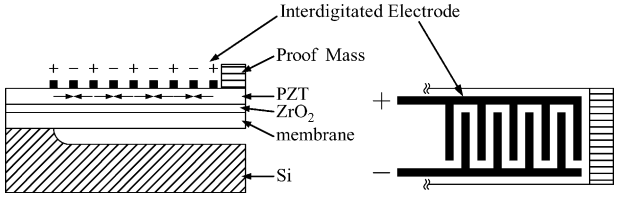


Fig. 3. Schematic of $d_{33}$ mode piezoelectric device.

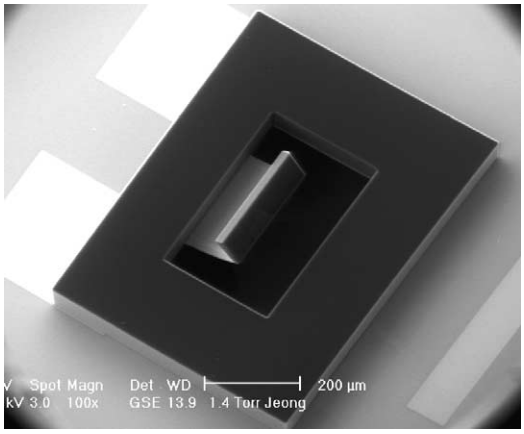


Fig. 4. SEM of the fabricated PMPG device with bond pads.

Ti and 200 nm Pt via e-beam evaporation and patterned using a lift-off procedure with the second mask. The thick photo resist, SU-8, is spin-coated on top of the existing layers and patterned with the third mask to create a proof mass. For a final step of releasing cantilever structure, a wet etching process such as KOH etch was initially used to bulk etch Si substrate. But serious stictions were observed and the KOH was found to attack the PZT layer. These problems are solved by employing $XeF_2$ vapor etching process where the PZT layer itself is used as an etch mask. $XeF_2$ has a high etch selectivity between Si and the other layers and does not attack PZT at all. [6] The PMPG device is fabricated as shown in Fig. 4.

### 3.2. Cantilever bow control

For the cantilever fabrication, we first fabricate PZT/$ZrO_2$/thermal $SiO_2$ structure. But this results in very severely curled cantilever beam, as shown in Fig. 5a. This bow of cantilever beam is due to the non-uniform residual stress distribution across the thickness, i.e. tensile stress in the top PZT layer and compressive stress in the bottom thermal $SiO_2$ layer. In order to reduce the bow of the cantilever beam, we tried to optimize the residual stress and mechanical properties of the membrane layer. This is because the function of $ZrO_2$ and $SiO_2$ layers are unique as buffer layers, so they are not exchangeable. The thermal $SiO_2$ membrane layer is replaced with PECVD $SiO_2$ and $SiN_x$. This selection is based on the data in Table 1 where the bow estimate is calculated by the beam theory [13–16]. The residual stress in Table 1 is estimated with Stoney's model [17] from a substrate curvature which is measured by a laser interferometric profilometer for each layer deposition, as shown in Fig. 6. Since the PZT layer is deposited repeatedly four times, the curvature is also measured for each subsequent deposition of PZT. The bow estimates lead us to reduce the bow by the two step approach as indicated in Fig. 7: changing the residual stress of the bottom layer from compressive to tensile and increasing its elastic modulus.

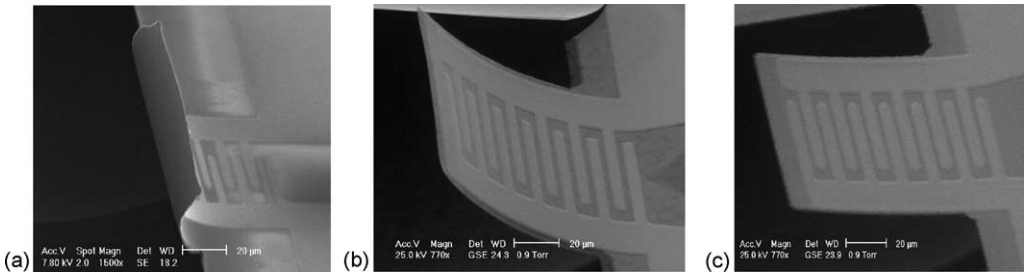


Fig. 5. SEM images of the stress-controlled cantilevers consisting of (a) PZT/$ZrO_2$/$SiO_2$(thermal), (b) PZT/$ZrO_2$/$SiO_2$(PECVD) and (c) PZT/$ZrO_2$/$SiO_2$(PECVD)/$SiN_x$.

Table 1
Mechanical properties and residual stresses of films deposited for the cantilever structure

| aa | PZT1 [12] | PZT 2 | PZT3 | PZT 4 | $ZrO_2$ [13] | $SiO_2$ [14] (thermal) | $SiO_2$ [14] (PECVD) | $SiN_x$ [15] |
|---|---|---|---|---|---|---|---|---|
| Elastic modulus [GPa] | 63 | 63 | 63 | 63 | 244 | 69 | 69 | 313 |
| Poisson ratio | 0.30 | 0.30 | 0.30 | 0.30 | 0.27 | 0.15 | 0.15 | 0.29 |
| Residual stress [MPa] | 630/610 | −115/−125 | 75/65 | 113/105 | 400/350 | −280/−330 | 35/−15 | 210/170 |

PZT number indicates the order in which the PZT film was deposited on top of the $ZrO_2$ layer.

Fig. 5b and c shows that our approach is appropriate. The first device, with thermal $SiO_2$ being the bottom layer in compression stress of about −300 MPa, has a severely curled cantilever as shown in Fig. 5a. In Fig. 5b, this bow is greatly diminished by depositing $SiO_2$ via PECVD, by which the compressive residual stress in the bottom layer is reduced to a few tens of MPa. In the smaller elastic modulus regime, however, even a small deviation from the target stress would result in a very large change of the cantilever curvature. Selecting a large elastic modulus actually gives us more robustness in controlling the bow. For this reason, a $SiN_x$ layer of high elastic modulus (313 GPa) and tensile stress (190 MPa) is selected as the membrane layer. A nearly flat cantilever beam is obtained as shown in Fig. 5c.

The curvatures of bow-controlled specimens (like those in Fig. 5b and c) are measured by the laser interferometric profilometer, assuming the profile is part of a circle. The measured curvatures are 2700 $m^{-1}$ (±250 $m^{-1}$) and 1780 $m^{-1}$ (±85 $m^{-1}$) for PECVD $SiO_2$ and $SiN_x$ bottom layers, respectively. The measured values are a little larger than predicted by the beam theory (1697 $m^{-1}$ for PECVD $SiO_2$ and 1339 $m^{-1}$ for $SiN_x$), but their tendency toward reducing bowing is well consistent. We think that the small deviation is due to the presence of residual-stresses built in the electrode layers (Pt and Ti) and additional release of the cantilever resulting from the undercut etching of the Si substrate.

### 3.3. Characterization

The PMPG device acts as an ac current generator in parallel with a complex output impedance. When the PMPG is mechanically vibrating at the resonant frequency, $\omega_n$, the PZT thin film experiences a time-varying change in mechan-

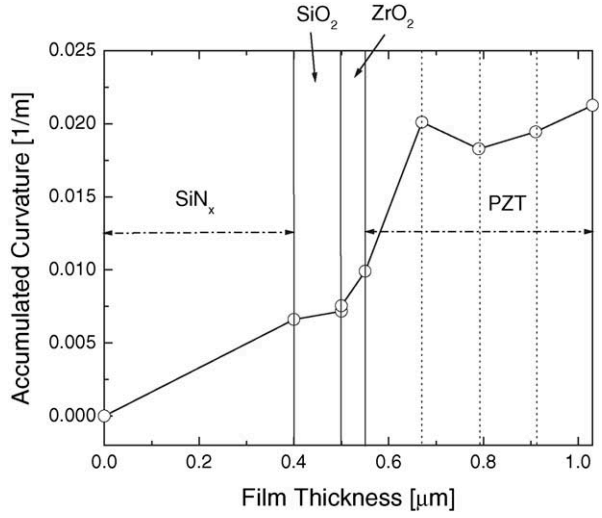


Fig. 6. Variation of the accumulated curvature of Si wafer with multilayer deposition of PZT/$ZrO_2$/$SiO_2$/$SiN_x$.

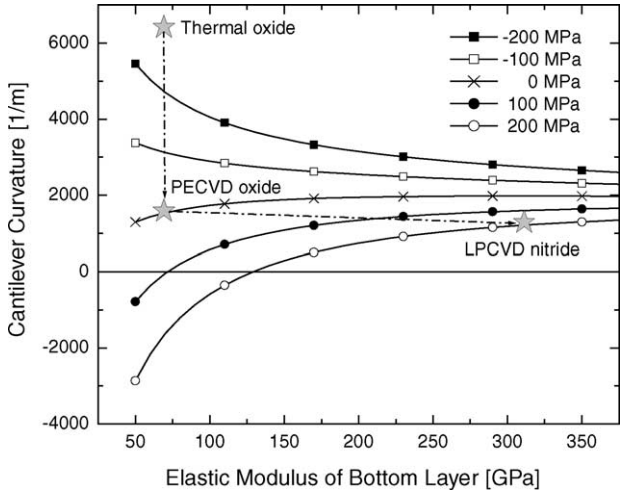


Fig. 7. Dependence of bow curvature of cantilever beam on elastic moduli and residual stresses of bottom layer.

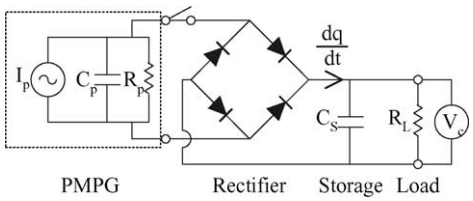


Fig. 8. Equivalent electrical model of the PMPG power system.

ical stress, $\sigma(t)$, alternating between tensile and compressive stress. This results in a time-varying generated charge within the PZT layer, which is the source of the ac current. Taking the first time derivative of the charge function, $Q(t)$, gives the ac current source, $I_P(t)$. A rectifying circuit and electrical storage capacitor are required for harvesting the electrical energy from each device (Fig. 8).

The fabricated device is packaged on a multiple pinned ceramic package (Fig. 4). Each device has two bond pads that connect the device to the measurement electronics and the external rectification circuitry, storage capacitor, and resistive load. The device is heated to 100 °C on a hot plate and poled at 90 V dc for 30 min. The temperature is then cooled down to a room temperature while maintaining the applied poling voltage.

The rectifying bridge circuit consists of four STMicroelectronics® 1N5711 small-signal Schottky diodes and a 10 nF mylar storage capacitor. These diodes are chosen specifically because, compared to most discrete components, they have the smallest forward voltage drop (approximately 0.2 V). This allows for the largest possible dc voltage to develop across the capacitance/load. The 10 nF mylar capacitor is chosen because it has a very low leakage current.

## 4. Results and discussion

The polarization properties of the PZT thin films are measured using the Radiant Technologies© RT-66A High Voltage Interface with Trek® Model 601C in the form of a *P–V* hysteresis curve. The measured spontaneous polarization ($P_s$), remanent polarization ($P_r$), coercive field, and dielectric constant are 50 μC/cm$^2$, 20 μC/cm$^2$, 38 kV/cm, and 1200$\varepsilon_0$, respectively.

In order to find out the resonance mode and tip displacement, the PMPG is directly excited with a ±3 V ac voltage source, scanning from 0 to 200 kHz. At the same time, the cantilever tip displacement was measured by a laser vibrometer. Fig. 9 reveals three resonant modes: 13.9, 21.9 and 48.5 kHz. The 13.9 kHz mode is the uniform bending mode which has the largest tip displacement amplitude. The 48.5 kHz is also a bending mode, but the beam bends both upward and downward in a snake-like fashion (the second harmonic), while the 21.9 kHz mode demonstrates a twisting type motion (torsional mode).

Having determined the first mode resonance, a piezoelectric shaker is then used to apply ambient vibration to the

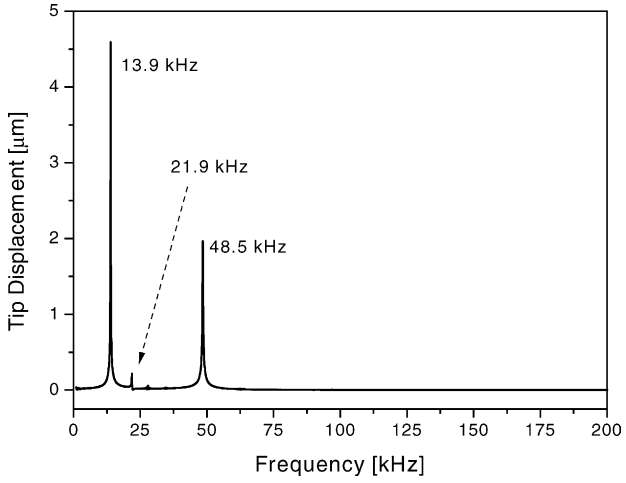


Fig. 9. Cantilever tip displacement with ac frequency.

PMPG at that frequency, 13.9 kHz. The magnitude of the base displacement is varied by changing the shaker drive voltage. Cantilever tip displacement and the corresponding closed-circuit charge (measured by a closed-circuit charge amplifier) are then measured against the input base displacement (Fig. 10). Here, base displacement is simply the displacement of the silicon substrate to which the micro cantilever is attached. The tip displacement is amplified by approximately 90 times over the base displacement during resonance. The amount of charge developed on the IDT electrode is approximately linear in proportion to the tip displacement. This is because the axial stress developed within the PZT layer also increases linearly with tip displacement. A maximum generated charge of 13.2 pC is measured at a maximum tip displacement of 2.56 μm. The charge increases linearly with tip displacement with a linearity coefficient of 4.14 pC/μm.

For the next set of base shaking experiments, the PMPG device is connected to a rectifying bridge circuit with a resis-

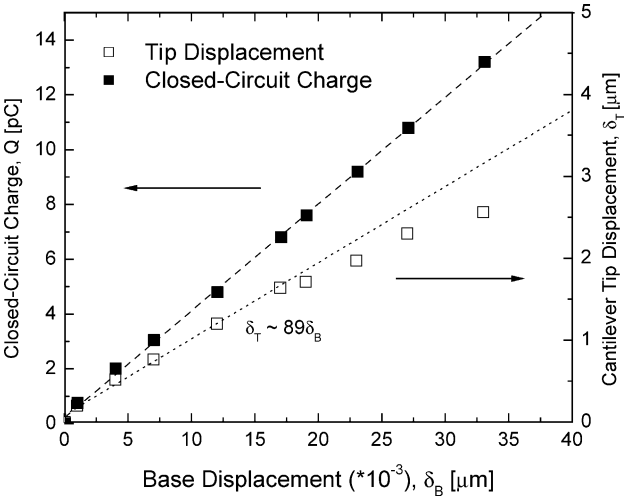


Fig. 10. Cantilever tip displacement and generated closed-circuit charge vs. base displacement.

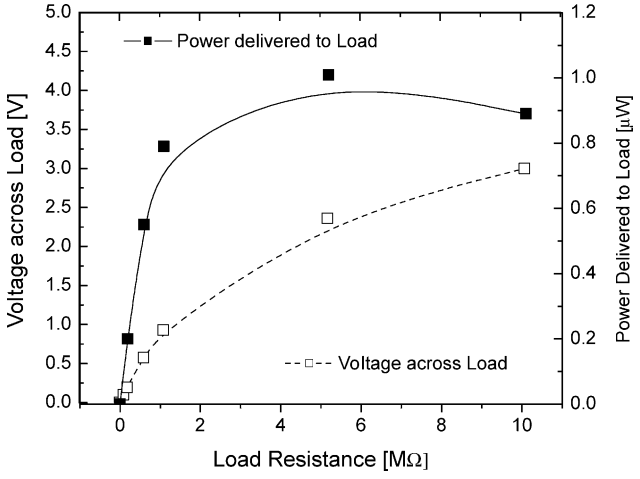


Fig. 11. Load voltage and power delivered to the load vs. load resistance at 13.9 kHz resonance.

tive load across the storage capacitor, as shown in Fig. 8. The load voltage is measured as a function of load resistance with a fixed base displacement magnitude of 14 nm at the shaking frequency of 13.9 kHz. Fig. 11 shows the load voltage and power delivered to the load. As expected, the load voltage increases with the increased load, up to 3 V at 10.1 MΩ. However, the power delivered to the load has a maximum value, 1.01 μW for the 5.2 MΩ load, after which the electrical power decreases with the increased load resistance. A 2.4 V dc voltage is measured at the 1.01 μW power level. Given the device area including the on-chip rectification and energy storage circuitry, this translates to an energy density of 0.74 mW h/cm$^2$, which compares favorably to the current lithium ion batteries. The storage capacitor charging and discharging times are approximately 0.2 and 0.3 s, respectively.

## 5. Conclusions

The ambient vibrational energy can be converted to electrical energy via the MEMS piezoelectric energy harvesting device and would power wireless MEMS sensors without keep replacing batteries. A thin film piezoelectric power generator is developed using a $d_{33}$ mode of piezoelectric transducer. It is designed to have a high open-circuit voltage to overcome the forward bias of the rectifying bridge. The process consists of the deposition of $SiN_x$ bottom membrane, $ZrO_2$ insulating layer, and PZT layer followed by RIE patterning, lift-off of Pt/Ti electrode layer, proof mass patterning, and $XeF_2$ release of the cantilever beam. By adjusting the residual stress and elastic modulus of the bottom membrane layer, a flat cantilever structure is fabricated. It is measured that the cantilever has three different resonance modes: two bending modes (13.9 and 48.5 kHz) and one torsional (21.9 kHz) mode. By exciting the cantilever at the first resonance frequency (13.9 kHz), a maximum dc voltage of 3 V is generated across the load (10.1 MΩ), and a maximum continuous electrical power of 1 μW is delivered to the 5.2 MΩ load. The corresponding energy density is 0.74 mW h/cm$^2$. Miniaturized wireless sensors would enable a large scale sustainable sensor network with the integrated energy harvesting devices demonstrated in this paper.

## Acknowledgements

Authors thank the Manufacturing Institute of MIT, the department of Mechanical Engineering of MIT, and Korea Institute of Metallurgy and Manufacturing for their support. J.-h. Jeong's work was supported by the post-doctoral fellowship program of Korea Science and Engineering Foundation.

## References

[1] S. Roundy, P.K. Wright, J. Rabaey, A study of low level vibrations as a power source for wireless sensor nodes, Comput. Commun. 26 (2003) 1131–1144.
[2] A. Chandrakasan, R. Amirtharajah, J. Goodman, W. Rabiner, Trends in low power digital signal processing, in: Proceedings of the 1998 IEEE International Symposium on Circuits and Systems, ISCAS'98, 1998.
[3] S. Meninger, J.O. Mur-Miranda, R. Amirtharajah, A.P. Chandrakasan, Vibration to electric energy conversion, IEEE Transact. VLSI Syst. 9 (2001) 64–76.
[4] W.R. Davis, N. Zhang, K. Camera, F. Chen, D. Markovic, N. Chan, B. Nikolic, R. Brodersen, A design environment for high throughput, low power dedicated signal processing systemsdkjdot, in: Proceedings of the IEEE Custom Integrated Circuits Conference, San Diego, CA, USA, 2001.
[5] C.W. Wong, Y. Jeon, G. Barbastathis, S.-G. Kim, Strain-tuning of periodic optical devices: tunable gratings and photonic crystals, Technical Digest of the 2002 Solid-State Sensor and Actuator Workshop, Hilton Head Island, SC, 2002, pp. 342–345.
[6] K. Hwang, M. Koo, S. Kim, High-brightness projection display systems based on the thin-film actuated mirror array (TFAMA), in: Proceedings of SPIE, Santa Clara, CA, USA, September 1998, pp. 171–180.
[7] P. Glynne-Jones, S.P. Beeby, N.M. White, Towards a piezoelectric vibration-powered microgenerator, IEE Proc. Sci., Meas. Technol. 148 (2001) 69–72.
[8] J. Kymissis, C. Kendall, J. Paradiso, N. Gershenfeld, Parasitic power harvesting in shoes, in: Proceedings of the Second IEEE International Conference on Wearable Computing ISWC, Pittsburgh, PA, USA, 1998.
[9] B. Xu, Y. Ye, L.E. Cross, J. Bernstein, R. Miller, Dielectric hysteresis from transverse electric fields in lead zirconate titanate thin films, Appl. Phys. Lett. 74 (1999) 3549–3551.
[10] J.J. Bernstein, J. Bottari, K. Houston, G. Kirkos, R. Miller, B. Xu, Y. Ye, L.E. Cross, Advanced MEMS ferroelectric ultrasound 2D arrays, in: IEEE 1999 Ultrasonics Symposium, Lake Tahoe, NV, 1999.
[11] R. Sood, Y.B. Jeon, J.H. Jeong, S.G. Kim, Piezoelectric micro power generator for energy harvesting, Technical Digest of the 2004 Solid-State Sensor and Actuator Workshop, Hilton Head, South Carolina, 2004.
[12] C.B. Williams, R.B. Yates, Analysis of a micro electric generator for microsystems, Sens. Actuators 52 (1996) 8–11.
[13] T.S. Low, W. Guo, Modeling of a three-layer piezoelectric bimorph beam with hysteresis, J. MEMS 4 (1995) 230–237.

[14] J.F. Lynch, C.G. Ruderer, W.H. Duckworth, Engineering Properties of Selected Ceramic Materials, American Ceramic Society, Columbus, Ohio, 1966.
[15] M. Fukuhara, A. Sanpei, Effects on high-temperature-elastic properties on α-/β-quartz phase transition of fused quartz, J. Mater. Sci. Lett. 18 (1999) 751–753.
[16] S. Sakaguchi, N. Murayama, Y. Kodama, F. Wakai, The Poisson's ratio of engineering ceramics at elevated temperature, J. Mater. Sci. Lett. 10 (1991) 282–284.
[17] Stoney G, The tension of metallic films deposited by electrolysis, Proc. Roy. Soc. (Lond.) A 82 (1909) 172–175.

## Biographies

**Y.B. Jeon** received the B.S. and M.S. degree in ceramic engineering from Yonsei University, Seoul, Korea, in 1988 and 1993, respectively, and the Ph.D. degree in materials science and engineering from KAIST, Korea, in 2001. He was a Postdoctoral Associate in the Micro and Nano Systems Laboratory at the Massachusetts Institute of Technology when the work in this paper was performed together with Prof. Sang-Gook Kim. He is currently working as a Principal Process Engineer and Account Technologist for Varian Semiconductor Equipment Associates, Inc., Lexington, MA.

**R. Sood** graduated from the Massachusetts Institute of Technology in 2003 with the B.S.E.E. and Masters of Electrical Engineering. Raj is currently working as a MEMS engineer for Polychromix, an advanced telecommunications technology company based in Wilmington, MA.

**J.-h. Jeong** received the Ph.D. degree in School of Materials Science and Engineering from Seoul National University, Seoul, Korea, in 2001. His research background has been the mechanical characterization and analysis for MEMS and thin-films materials. He joined Massachusetts Institute of Technology (MIT) in 2003 as a Postdoctoral Associate until 2004. Dr. Jeong is currently working for the Korea Institute of Science and Technology as a senior research staff. His current research interests include a piezoelectric power generation, a carbon nanotube growth and its assembly, and a phase change nonvolatile random access memory.

**S.-G. Kim** received the Ph.D. in mechanical engineering from MIT in 1985. From 1985 to 1986, Professor Kim was a manufacturing manager at Axiomatics Corp. in Cambridge, MA. He then joined the Korea Institute of Science and Technology in 1986 as a senior research staff until 1990. He joined Daewoo Corporation, Seoul, Korea in 1991, as a general manager at the Corporate Chairman's Office. He directed the TMA (Thin film Micro mirror Array) Research Center at Daewoo Electronics and was promoted to a corporate director and corporate executive director in 1995 and 1998, respectively. He joined the faculty at the MIT in September 2000. His research interest is now on multi-scale systems design and nanomanufacturing, carbon nanotube assembly, piezoelectric energy harvesting and portable energy.